Colored dual-functional photovoltaic cells

2016 J. Opt. 18 064003

(http://iopscience.iop.org/2040-8986/18/6/064003)

IOP Publishing Journal of Optics
J. Opt. 18 (2016) 064003 (11pp) doi:10.1088/2040-8978/18/6/064003

Colored dual-functional photovoltaic cells

Kyu-Tae Lee[1,4], Jae Yong Lee[1,5], Ting Xu[1,6], Hui Joon Park[2,3] and L Jay Guo[1]

[1] Department of Electrical Engineering and Computer Science, The University of Michigan, Ann Arbor, MI 48109, USA
[2] Division of Energy Systems Research, Ajou University, Suwon 443-749, Korea
[3] Department of Electrical and Computer Engineering, Ajou University, Suwon 443-749, Korea

E-mail: huijoon@ajou.ac.kr and guo@umich.edu

Received 30 January 2016, revised 16 March 2016
Accepted for publication 17 March 2016
Published 13 April 2016

Abstract

In this article, we review our recent efforts on multi-functional photovoltaic (PV) cells that can produce desired reflective, transmissive, or neutral colors, by controlling light interaction with semiconductors and electrode structures in a desired manner. The PV cells integrated with plasmonic color filtering schemes using subwavelength gratings, and other approaches exploiting photonic resonances in an optical nanocavity consisting of highly absorbing semiconductor media are described. For further enhancement of optical and electrical performance characteristics of the multi-functional PV cells, possible difficulties and the outlook for future work are discussed.

Keywords: solar cells, color filters, surface plasmon, nanostructures, nanocavity

(Some figures may appear in colour only in the online journal)

1. Introduction

Converting sunlight into electricity has been regarded as one of the most effective ways to harvest inexhaustible solar energy. With the development of new photovoltaic (PV) materials, processings, and device engineering, the power conversion efficiency has been continuously improved. Existing PV platforms have employed a very thick semiconductor layer that is essential to completely absorb the entire solar spectrum for maximum electric power generation. Having such a thick semiconductor layer, however, results in an unappealing black appearance. Consequently, the traditional PV panels have been largely deployed on limited areas such as rooftops of buildings so a large amount of building surfaces and interiors for light energy harvesting is wasted.

In recent years, rapid progress has been made in developing colored and semitransparent PV devices, which can be incorporated with building envelopes to harvest sunlight, thereby opening up diverse potential applications, including building-integrated PV (BIPV) and energy-efficient display systems. Various device configurations have been adopted to demonstrate the multi-functional PV cells. Dye-sensitized PV (DSPV) has gained growing attention because semi-transparent PV cells with desired aesthetic functionalities can be achieved by using dyes for different colors. However, limited dye materials have restricted color variation and thus tunability. Another challenge arises from the inherent mesoporous structures in the DSPV that can cause the light scattering, thus leading to blurred images [1, 2]. Structural color filters based on a plasmonic resonance were also integrated with organic PV (OPV) to create desired reflective colors while generating electric power. In this device structure, the color can be easily tuned by varying a period of metallic gratings, which can excite surface plasmon resonances (SPR) at different wavelengths of visible light [3]. Despite such easily tunable characteristics, the property of the SPR is inherently dependent on the angle and polarization state of incident light, which is due to the momentum matching condition necessary to excite the SPR by the subwavelength gratings. These are critical issues to be addressed as sunlight comes from a wide range of incident angles with unpolarized characteristics. Moreover, patterning the gratings at the

[4] Current address: Department of Materials Science and Engineering, The University of Illinois at Urbana-Champaign, Urbana, Illinois 61801, USA.
[5] Current address: 3M Corporate R&D, 3M, St. Paul, Minnesota 55144, USA.
[6] Current address: College of Engineering and Applied Sciences, Nanjing University, Nanjing, People's Republic of China.

subwavelength scale involves complex lithographic techniques, thus restricting their potential for large-scale applications. To address the above challenges, pattern-free, thin-film amorphous silicon (a-Si) semiconductor based optical nanocavity featuring ultrathin cavity thickness that is much thinner than the wavelength of incident light was directly embedded into the PV device structure [4, 5]. Strong interference behaviors in ultrathin semiconductor films were exploited to create the photonic resonance at visible frequencies and therefore the desired colors. The resulting colors are insensitive with respect to both the incident angle and the polarization, which is primarily attributed to the reduced phase shift of light propagating through the ultrathin cavity layer that cancels with phase changes upon reflecting from the metal surface [6–9]. Creating the resonance in semiconductor materials that strongly absorb visible spectrum of light depending on the bandgap of the materials, however, always yields the resonance with a broad bandwidth, thus causing low color purity. Additionally, the optical absorption is limited by the ultrathin photoactive layer thickness and hence the corresponding power conversion efficiency is limited. As an alternative approach to enhance both optical and electrical performances of the colored and semitransparent PV cells, the conventional Fabry–Pérot (F–P) cavity was incorporated with the cathode of various PV devices, including organic and perovskite semiconductors [10–12]. We note that other perfect light absorption schemes, which include the plasmonic resonances, plasmonic near-field coupling effects in the metallic nanoparticles, coupled metal film systems and multicavity resonances, can also be incorporated with any PV material system to create the colored PV cells and further improve the performance characteristics [13–22].

In this article, we summarize our recent progress toward achieving multi-functional PV devices with desired semitransparent color generation in various PV material systems. We conclude with a discussion of the challenges and potential solutions for further improving the performance of the multifunctional PV devices.

2. Plasmonic color filters integrated with OPV

With the development of nanofabrication and characterization technologies, the optical resonance effects in various 1D and 2D metallic nanostructures such as SPR, a resonant oscillation of electrons at metal–dielectric interfaces, have been widely investigated to exploit them to structural color generation [23–27]. Different with conventional pigment-based color filtering system, the structural colors from those plasmonic nanostructures can be easily tuned by their dimension and geometry. Meanwhile, the applicability of those metal nanostructures to semitransparent electrodes for organic optoelectronic devices such as OPV and organic light-emitting diodes has been successfully demonstrated [28, 29]. For example, precisely designed 1D metallic nanogratings have shown the comparable optical transparency and electrical conductivity to the conventional indium tin oxide (ITO) electrode [30, 31]. This potential dual functionality of metallic nanostructures paved the way for the multifunctional device working as color filters as well as PV cells [3]. The periodic gold (Au) nanogratings in figure 1 act not only as nanostructures to modulate incident light to generate different colors but also as semitransparent electrodes for the OPV cells. To construct polarization insensitive color filters, different design strategies for the transverse electric (TE) and transverse magnetic (TM) waves were utilized. By constructing the device to have metal–dielectric–metal F–P cavity structure, the resonance wavelength under TE polarized light (the *E*-field is parallel to the Au nanograting direction) could be controlled with the thickness of a dielectric layer consisting of, such as hole transporting layer poly(3,4-ethylenedioxythiophene):poly(styrenesulfonate) (PEDOT:PSS) and organic semiconductors poly(3-hexylthiophene):[6,6]-phenyl C_{61} butyric acid methyl ester (P3HT:PCBM), which is sandwiched by an Au nanograting layer and a continuous thick Al film functioning as electrodes. Furthermore, TM waves (the *E*-field is perpendicular to the Au nanograting direction) could be coupled to the SPR mode through the subwavelength Au nanograting structures, so the resonance wavelength under TM polarized light could be controlled by the period of the Au nanogratings. The resultant reflectance type color filtering behaviors for cyan (C), magenta (M) and yellow (Y) are shown in figure 1(a). The periodic Au nanograting structures in this approach were fabricated using nanoimprint lithography to produce large-area electrodes onto which the OPV cells can be easily fabricated. All three colored devices showed reasonable PV performances as shown in figure 1(b2).

3. Ultrathin a-Si PV cells with reflection/transmission colors

Although various structural color filters, which rely on the SPR or guided mode resonances, can be integrated with any kinds of the PV systems, their optical properties are intrinsically angle dependent as the subwavelength gratings need to be involved to excite these resonances, thus dramatically limiting their potential in diverse applications. To address the aforementioned issues, a new optical nanocavity exploiting strong interference effects in highly absorbing semiconductor films with the ultrathin cavity thickness as compared with the wavelength of incident light was incorporated as shown in figure 2(a) [5]. The nanocavity consists of the semiconductor materials (e.g. a-Si) on a metallic substrate, which exploits an nontrivial phase shift occurring upon reflections at the interface between the semiconductor and metal, and significantly reduced propagation phase shift, creating the resonance in the ultrathin cavity layer that is much thinner than the wavelength of incident light [6–9]. Increasing the thickness of the photoactive layer leads to the resonance formed at longer wavelengths and hence the resulting color is shifted from the yellow to the cyan as illustrated in figure 2(b). As the conventional a-Si PV mostly adopts a p–i–n structure configuration where the thickness of the n- and p-doped regions is around 50 nm, which is too thick to form the resonance in the

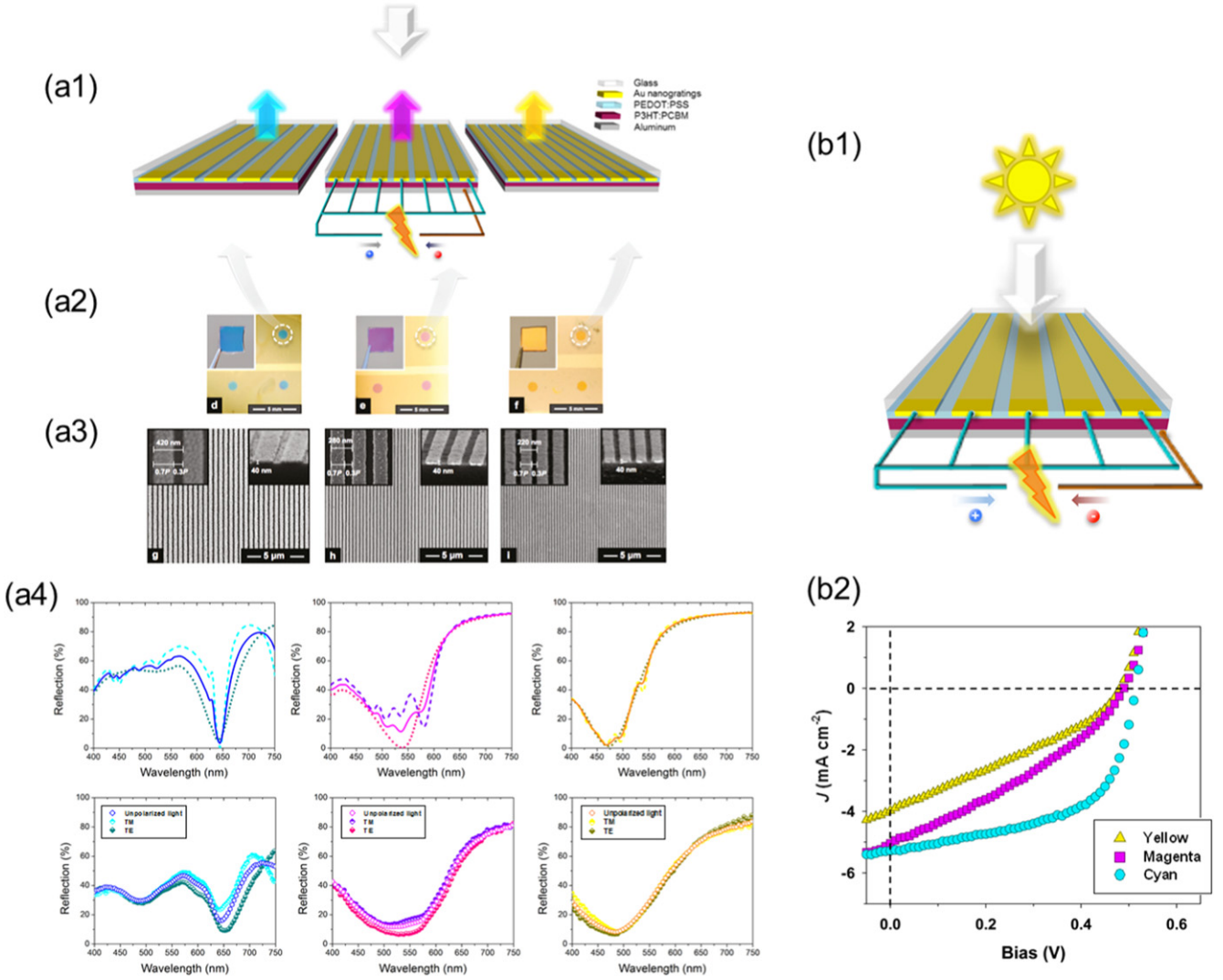

Figure 1. Characteristics of dual-function devices as (a) color filters (left, center and right cases are cyan, magenta and yellow, respectively.) and (b) PV cells: (a1) schematics of dual-function devices as color filters, (a2) photographs of dual-function devices having a 1 mm diameter circular shape. The inset images are the large-area version having about 1 cm size. (a3) Scanning electron microscope (SEM) images of Au nanogratings. The left and right inset images are the high magnification top and tilted views, respectively. The P in the left inset image represents the period of Au nanogratings. (a4) Color filtering behaviors in dual-function devices. The top three spectra are calculated by rigorous coupled-wave analysis (RCWA) simulation and bottom three spectra are experimentally measured. (b1) A schematic of a dual-function device showing photovoltaic property. (b2) *J*–*V* plots of dual-function devices. All data were measured at AM1.5 G with an intensity of 100 mW cm^{-2}. Circle, square, and triangle symbols represent the devices showing cyan, magenta, and yellow colors, respectively. Reproduced with permission [3]. Copyright 2011, American Chemical Society.

highly absorbing semiconductor media at visible frequencies, a new hybrid PV device structure, which utilizes organic and inorganic interfacial layers to replace the n- and p-doped layers, was employed [32]. Photogenerated holes are efficiently transported through vanadium pentoxide (V_2O_5) layer that has a high work function, while the efficient extraction of photogenerated electrons to a cathode is enabled by using indene-C_{60} bisadduct (ICBA) whose level of a lowest unoccupied molecular orbital is matched well with the conduction band of the a-Si material [33, 34]. Bis-adduct fullerene surfactant (C_{60} surfactant) was then deposited, which lowers the silver (Ag) work function and therefore creates an ohmic contact at the cathode [35]. For the metallic film, Ag was chosen due to its highest reflections and lowest absorptions among metals in the visible range. In this design, an additional top metallic mirror was placed on top of the ultrathin undoped a-Si photoactive layer in order to provide a high reflectivity that is needed to create the resonance with higher *Q*-factor, which improves the color purity. As the reflection from the surface of the top metal is fairly strong, a wide-bandgap semiconductor, tungsten trioxide (WO_3), was pre-deposited to serve as an anti-reflection (AR) coating layer. Such dielectric–metal–dielectric (DMD) electrodes have been extensively studied, showing enhanced transmission efficiency with a low series resistance as compared to ITO electrodes widely used in most electronic devices [4, 5, 36–39]. Removing the doped layers allows the intrinsic a-Si photoactive layer to be ultrathin, which is an order of

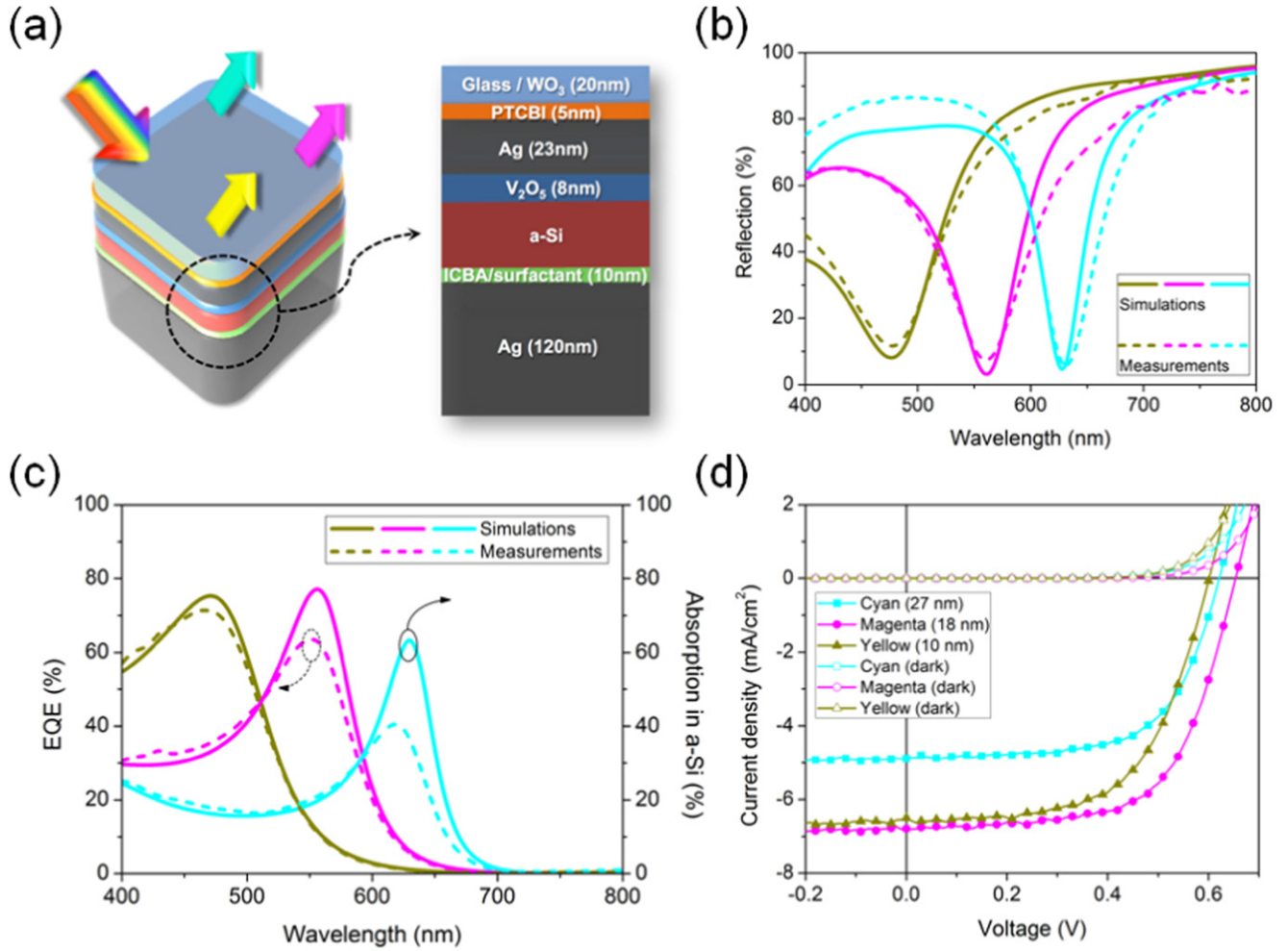

Figure 2. (a) The device structure of the dual-function hybrid PV cells. The cathode comprises a thick Ag layer and an organic layer (i.e. ICBA), and a dielectric-metal structure is used for the anode. Between the two electrodes is an ultrathin, undoped a-Si layer. (b) Calculated (solid lines) and measured (dotted lines) reflection profiles of the cyan, magenta, and yellow (CMY) devices at normal incident angle. The thicknesses of the a-Si layer for the CMY colors are 27 nm, 18 nm and 10 nm, respectively, given fixed thicknesses of all the other layers as shown in figure 2(a). (c) Measured external quantum efficiency (EQE) spectra and calculated absorption spectra in the a-Si layers for three individual colors: CMY. (d) *J*–*V* characteristics of individual colored cells under both AM1.5 illumination and dark conditions. Reproduced with permission [5]. Copyright 2014, Nature Publishing Group.

magnitude thinner than the traditional a-Si PV, so that the resonance in the visible wavelength regime can be formed to produce the desired colors. In addition to the color generation, such a dopant-free device structure with the ultrathin intrinsic photoactive layer enables a remarkable suppression of photo-carrier recombination, showing very high internal quantum efficiency, which can be confirmed by the fact that simulated absorption spectra in the photoactive layer are in good agreement with measured external quantum efficiency (EQE) (figure 2(c)). This is because the photoactive layer thickness is much thinner than a charge diffusion length of the a-Si material, thus implying that a vast majority of the photons are efficiently absorbed in the undoped a-Si photoactive layer and hence contribute to the electricity generation. In figure 2(d), current density–voltage (*J*–*V*) characteristics of the colored a-Si PV devices are presented showing that ~3% of the power conversion efficiency was achieved from a magenta colored PV cell whose photoactive layer thickness is only 18 nm that is an order of magnitude smaller than that of the traditional a-Si PV cell, a result of the optical resonance effect. The use of the ultrathin cavity layer ensures greatly reduced propagation phase shift as in a typical F–P cavity. This small propagation phase is further canceled out by the negative phase-shift of light reflecting from the semiconductor/metal interface at various incident angles [9], leading to an angle invariant color that is highly desirable to the PV applications as described in figure 3.

Utilizing optically transparent electrodes at the cathode, the dual-functional PV device is capable of producing semi-transparent colors as well [4]. To achieve this goal, the DMD electrode was used at both the anode and cathode as can be seen from the schematic diagram exhibited in figure 4. However, the purity of generated colors is relatively low, which is attributed to the resonance with a broad bandwidth, resulting from the absorption of the semiconductor film. Moreover, the light intensity reflected from the DMD cathode is relatively weak, thus resulting in lower efficiency less than 2%. In section 5, a new approach will be discussed to improve

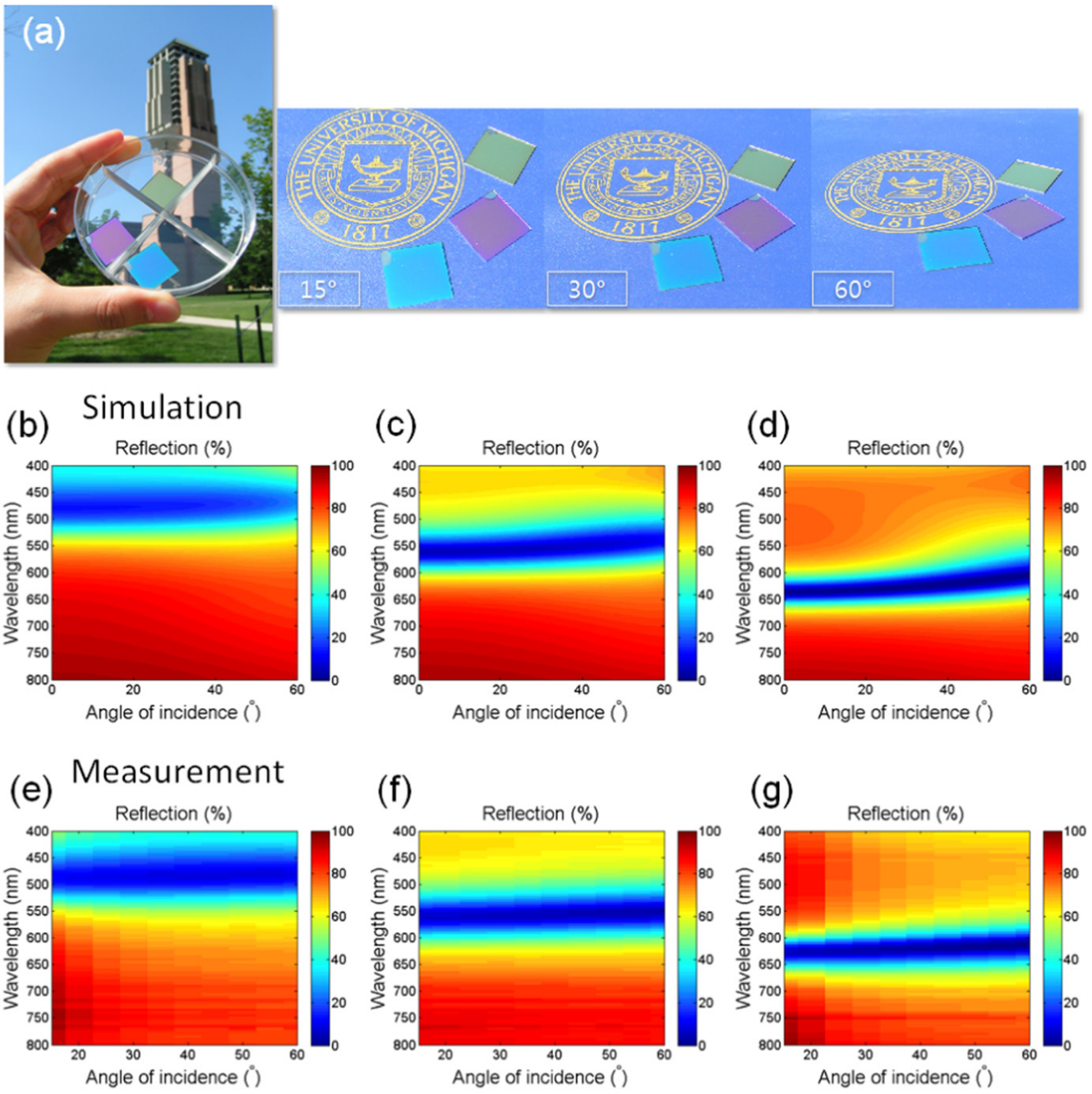

Figure 3. (a) Optical images of the fabricated devices displaying vivid CMY colors. The colored cells clearly present angle invariant characteristics at large angles of incidence (15°, 30°, and 60°). (b)–(d) Dispersion curves (for p-polarized light) obtained through simulation (transfer matrix method) for Y (10 nm), M (18 nm), and C (27 nm), respectively. The flat dispersion curves indicate that the devices have low sensitivity to the angle of incidence ranging from 0° to 60°. The color maps represent the intensity values for the reflected light. (e)–(g) Experimental dispersion curves measured using a spectroscopic ellipsometer and corresponding to those in (b)–(d). Reproduced with permission [5]. Copyright 2014, Nature Publishing Group.

both optical (i.e. color purity) and electrical performance characteristics (i.e. power conversion efficiency) of the colored and semitransparent PV cells.

4. Neutral-colored, semitransparent a-Si PV cells

There has been growing interest in semitransparent PV cells that enable a wide variety of applications, such as BIPV, PV curtains, and power-generating windows. Various approaches using organic and perovskite PV systems have been suggested and experimentally demonstrated to achieve the semitransparent characteristics while generating electric power [40–45]. In this section, we present a three nanometer thick a-Si PV operation for neutral-colored, semitransparent power-generating window applications, which previous technology could not resolve. The ultrathin a-Si PV cell utilizes inorganic (V_2O_5)/organic (ICBA) hybrid charge

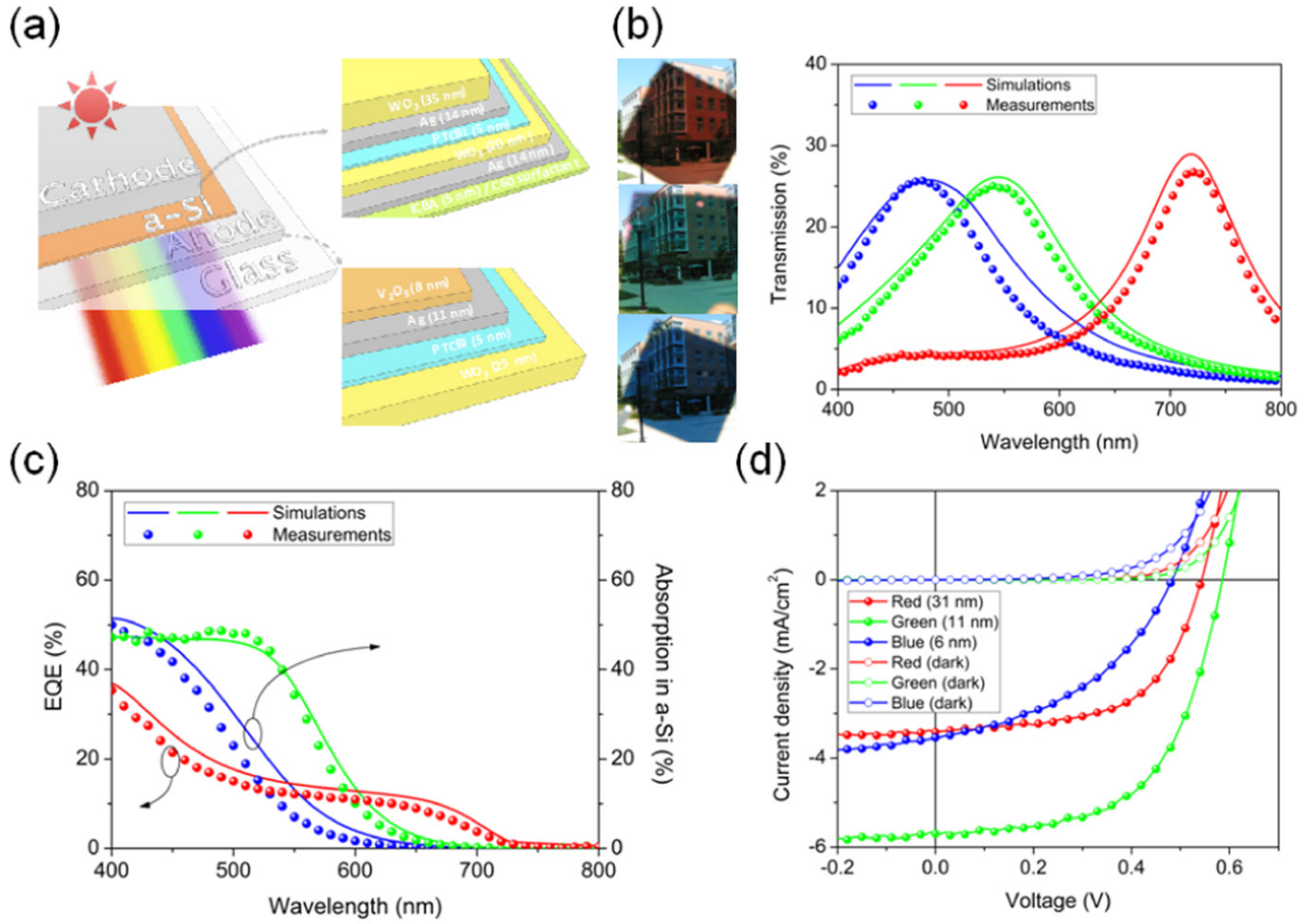

Figure 4. (a) Schematic representation of the semitransparent, colored a-Si PV device structure. The structure comprises cathode, anode, and ultrathin undoped a-Si. The cathode is composed of DMD and organic layers, and only DMD structure for the anode. The ultrathin a-Si layer thickness is 6, 11, and 31 nm for blue (B), green (G), and red (R), respectively. (b) Photographs of distinct B, G, and R colors by the fabricated devices, and calculated and measured transmission spectra of individual colors (B, G, and R) at normal incidence. (c) Comparison of calculated incident light absorption profiles by ultrathin a-Si layer and measured EQE spectra for three different types of devices (B, G, and R). (d) *J–V* characteristics of the hybrid cells under AM1.5 illumination and dark conditions. Reproduced with permission [4]. Copyright 2014, Nature Publishing Group.

transport layers instead of the conventional p- and n- doped regions as discussed in the previous section. With 3 nm thick a-Si in such hybrid cells, we could eventually achieve power-generating window devices with over 67% of optical transparency. The explored optical characteristics potentially enable the nanometer-thick hybrid cells to not only generate electric power but efficiently block ultraviolet (UV) lights since the a-Si material strongly absorbs shorter wavelengths.

Schematic diagram of the neutral-colored, semitransparent a-Si hybrid PV cell structure fabricated on ITO substrates is shown in figure 5(a). The structures have V_2O_5 for transporting holes and ICBA for electrons. Followed by ICBA, another 5 nm thick C_{60} surfactant is used to reduce the work function of the Ag electrode, thus offering the ohmic contact between Ag and the electron transport layer. The cell with 3 nm thick intrinsic a-Si photoactive layer shows the highest transparency. To achieve the semitransparent PV devices, the top Ag cathode is designed to be around 13 nm and finally covered by the optically transparent dielectric material, WO_3. The WO_3 capping layer provides a protection of the Ag electrode as well as improved transmission efficiency of the PV cells by reducing the reflection from the thin Ag film cathode. We should point out a recent development that by introducing small amount of aluminum (Al) during the Ag deposition, highly transparent, ultrathin (e.g. 8 nm) and smooth Ag films can be obtained with high stability [46, 47], which can benefit the semitransparent PV applications. The device fabrication is similar to the colored a-Si based PV described above, where V_2O_5, Ag, and WO_3 are thermally evaporated and the intrinsic a-Si material is deposited using a plasma-enhanced chemical vapor deposition. ICBA and C_{60} surfactant are spin casted.

The electrical performance of the semitransparent hybrid PV device is characterized by performing *J–V* measurement. Even with a highly transparent property showing over 67% of transmission averaged from 450 nm to 700 nm, our hybrid cells still generate electricity under AM 1.5 simulated light with the suppressed dark current as shown in figure 5(b). The hybrid cells provide around 1.0 mA cm^{-2} and 0.35 V, J_{sc} and V_{oc}, respectively.

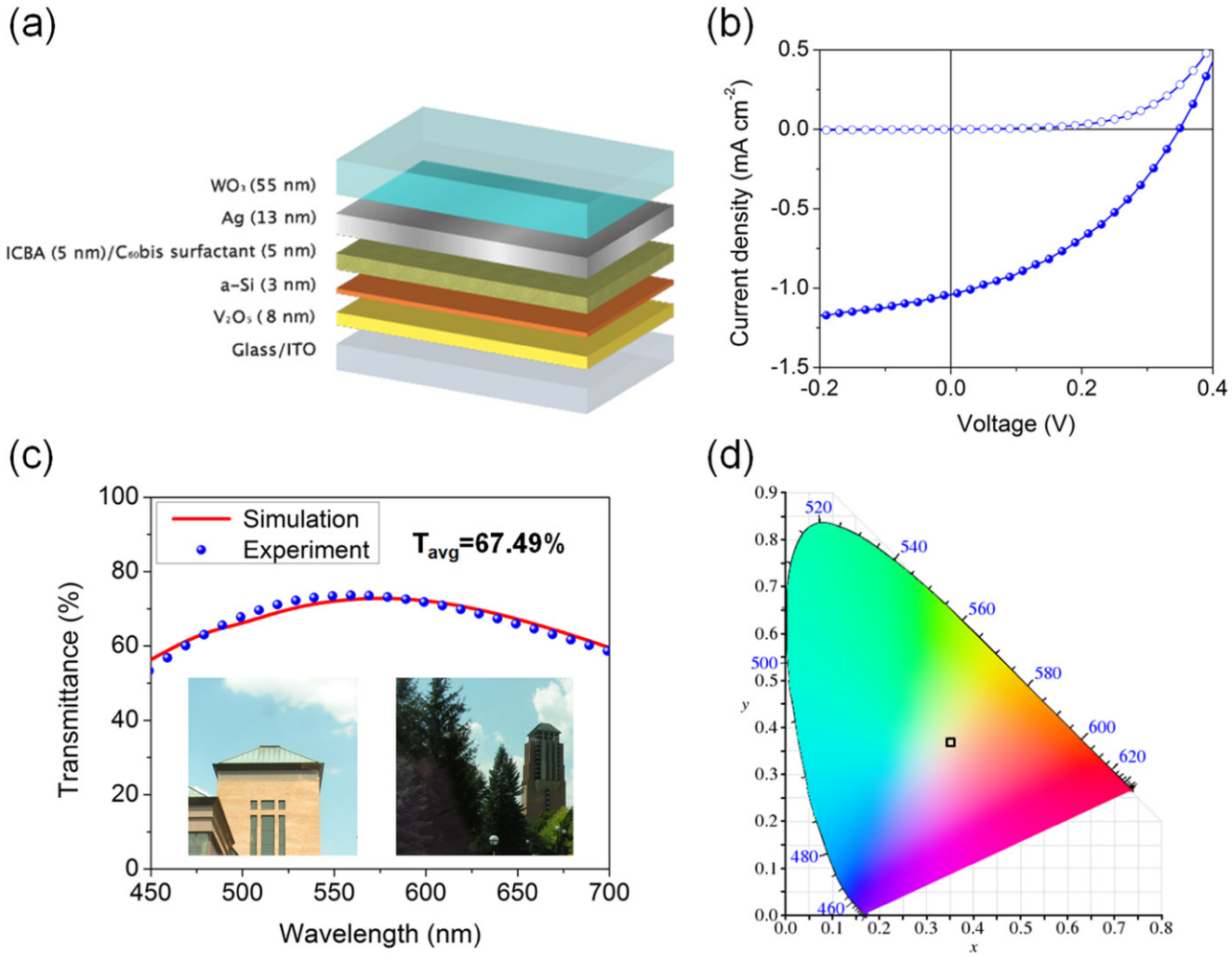

Figure 5. (a) Schematic illustration of the neutral-colored semitransparent a-Si hybrid PV cell. A cathode comprises optically transparent Ag (13 nm)–WO_3 (55 nm) with organic electron transport layers, and ITO with V_2O_5 (8 nm) hole transport layer for an anode. Between the two electrodes, a few nanometer a-Si is located. (b) *J*–*V* characteristics of the semitransparent hybrid cell are studied for electric power generating performance under AM 1.5 illumination and dark condition. (c) Calculated and measured optical transmission spectra that are in excellent agreement, both of which show ~67% of average transmission of visible light. Inset shows photographs of the fabricated hybrid cell with 3 nm thick a-Si photoactive layer exhibiting a semitransparent property, thus being able to clearly see objects through our sample. (d) The CIE 1931 chromaticity diagram evaluating transparency by giving the color coordinate at (0.358, 0.360), close to the coordinate of the white light (0.33, 0.33).

We also investigate optical properties of the semitransparent a-Si hybrid PV cells. Benefited by a few nanometer-thick a-Si hybrid cells, we can design fairly transparent PV structures by incorporating metal–dielectric transparent cathode instead of conventional thick metal film. 3 nm of the a-Si layer was utilized for the photoactive layer along with the cathode of the Ag and WO_3, 13 nm and 55 nm, respectively. Figure 5(c) shows the optical transmission spectrum calculated by the transfer matrix method featuring a flat spectrum in the visible band, which agrees very well with the experimentally measured transmission from the fabricated structures, along with photographs of the fabricated hybrid PV devices under outdoor sunlight as shown in the inset of figure 5(c) clearly showing high level of transparency. The resulting transmission spectrum exhibits 67.49% of the average transmission (AVT) of visible lights ranging from 450 nm to 700 nm, which is much higher than the AVT presented in the previous works. Such flat and broad transmission characteristics are primarily due to the resonance formed in a cavity consisting of a highly absorptive material (a-Si) with an extremely thin cavity length [6–9] and low quality factor (*Q*-factor) arising from the weak reflections at the interfaces (i.e. V_2O_5/a-Si and thin Ag/C_{60} surfactant). In addition, we calculate the color coordinate (x, y) under AM 1.5 illumination, which is depicted on the CIE 1931 chromaticity diagram to estimate the transparency perception of the 3 nm thick a-Si hybrid PV cell as shown in figure 5(d). The calculated color coordinate is (0.358, 0.360), demonstrating good transparency that is fairly close to the white light (0.33, 0.33).

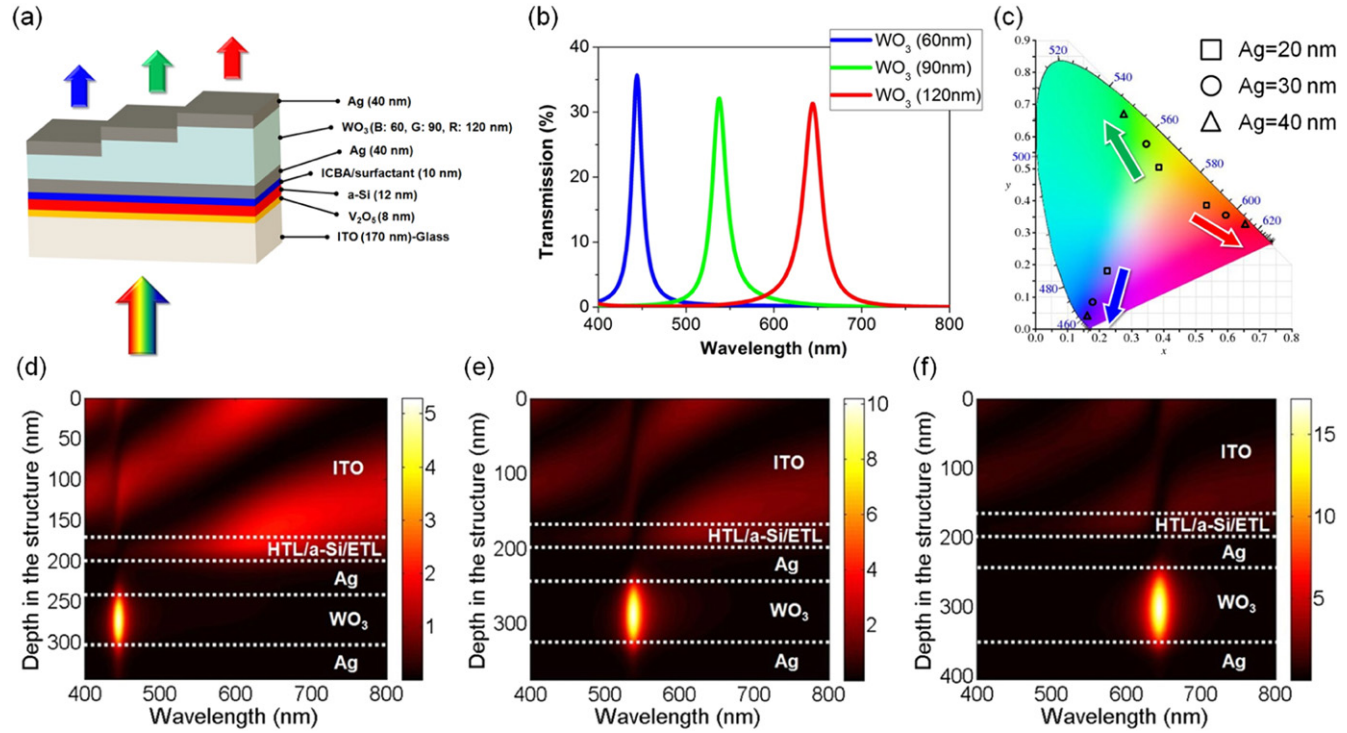

Figure 6. (a) Schematic diagram of the colored semitransparent a-Si/organic hybrid PV employing a MDM microcavity as a cathode. (b) Simulated transmission profiles of RGB colored PV devices at normal incidence. Varying the thickness of the WO_3 film inside the cathode enables the semitransparent colors to be tuned. 120, 90, and 60 nm of the WO_3 layer are used for producing the RGB transmission colors, and the corresponding resonances are 645 nm, 540 nm, and 445 nm, respectively. (c) Color coordinates (x, y) of the colored semitransparent PV devices with different thickness of the Ag reflector inside the microcavity-integrated cathode described on the CIE 1931 chromaticity diagram. By increasing the Ag mirror thickness, the resulting color coordinates approach the edge of the diagram, which signifies noticeably enhanced color purity. (d)–(f) Normalized intensity distributions of the optical field of the colored PV devices creating (d) blue (WO_3 = 60 nm), (e) green (WO_3 = 90 nm), and (f) red (WO_3 = 120 nm) transmission colors. The strong resonance effects (bright color) in the WO_3 cavity layer are observed at 445, 540, and 645 nm for the blue-, green-, and red-colored PV cells, respectively. These resonance wavelengths match well with the peak positions of the spectral transmittance curves depicted in figure 6(b). At the resonance wavelength, a portion of incoming solar radiation needs to be transmitted to produce the colors, which cannot be absorbed by the PV cells for electric power generation, thus exhibiting the weak field concentration (dark color) in the a-Si film. In contrast, the strong optical field in the a-Si layer at off-resonance wavelengths is observed, which results from the strong reflections from the Ag mirror back toward the photoactive layer, suggesting that the majority of incident light could be efficiently harvested by the PV cells. Reproduced with permission [11]. Copyright 2015, IEEE.

5. Microcavity-integrated colored, semitransparent PV cells

As described in a section 3, the transmission spectrum of the ultrathin lossy medium-based colored and semitransparent a-Si PV cells contains a large amount of off-resonance components of visible light, which leads to low purity of the transmission colors. An alternative is to exploit the traditional optical cavity comprising the optically transparent medium (i.e. WO_3) with the wavelength-scale thickness at the cathode [11]. As depicted in figure 6(a), the device structure in this work starts from the ITO electrode instead of the DMD electrode because the color is generated only from the microcavity-embedded cathode, ensuring that the color purity is not degraded by another resonance that arises from the ultrathin a-Si photoactive layer. For all transmission colors, the thickness of the undoped a-Si layer is designed to be 12 nm, which shows the maximum optical absorption in the photoactive layer. This is because shorter wavelength regions of visible light can be efficiently harvested by the a-Si material that has a strong absorption coefficient at blue regimes (i.e. 400–550 nm). In addition to the strong absorption characteristics of the a-Si material at the shorter wavelengths, the spectrum ranging from 550 nm to 650 nm is strongly absorbed in the a-Si layer by creating the resonance in the ultrathin photoactive layer, which is enabled with 12 nm thickness. We note that the a-Si material has a negligible absorption performance at longer wavelengths beyond 700 nm because of the bandgap. The semitransparent colors can be tuned by simply altering the thickness of the optical spacer layer, WO_3, as can be seen from figure 6(b) exhibiting calculated transmission spectra at normal incidence. It is obvious that the spectrum has a sharp resonance transmission with greatly suppressed off-resonance wavelengths, which is resulting from the strong reflections of the thick Ag mirror (40 nm) in the optical cavity, thus providing high Q-factor. This leads to significantly improved color purity as presented in figure 6(c) showing that the chromaticity coordinates (x, y) from the simulated spectral transmission curves (figure 6(b)) are evaluated and then represented

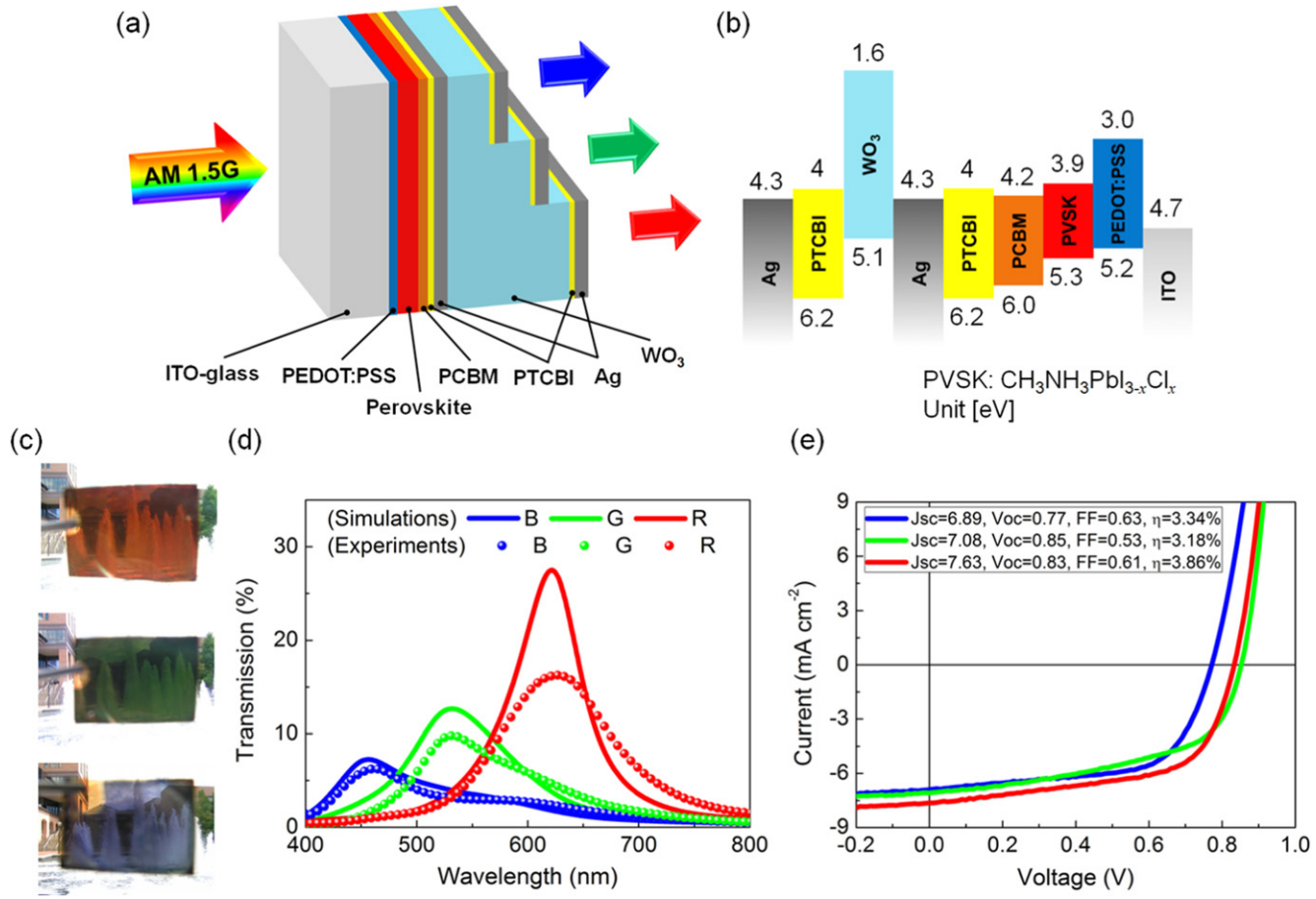

Figure 7. (a) Schematic view of the colored, semitransparent perovskite PV device employing a microcavity consisting of a dielectric medium sandwiched by optically thin metallic layers in the cathode side. The desired transmission RGB colors can be tuned by simply varying the thickness of the dielectric layer in the microcavity. Each layer's thickness is as follows: PEDOT:PSS = 50 nm, perovskite = 80 nm, PCBM = 60 nm, Ag = 20 nm, PTCBI = 8 nm, WO_3 = 65 (blue), 85 (green), 115 nm (red). (b) Energy level diagram of each layer in the device structure. The energy level is relative to the vacuum level. PVSK represents $CH_3NH_3PbI_{3-x}Cl_x$ and the unit is electron volts (eV). (c) Optical photographs of fabricated colored PV devices. The background image can be clearly seen through our fabricated samples with RGB colors. (d) Simulated and measured spectral transmittance curves of the colored, see-through perovskite PV devices at normal incident angle. Increasing the thickness of the WO_3 layer in the microcavity cathode allows the resonance (i.e. transmission peak) to be shifted toward the longer wavelengths. The resonances at 630 (red), 540 (green), and 450 nm (blue) are attained by WO_3 layer thicknesses of 115 nm, 85 nm, and 65 nm, respectively. As the wavelength increases, the difference between the simulated and measured transmission spectra becomes large. Due to the negligible absorption of the perovskite photoactive layer at longer wavelengths, the red colored PV cell has the sharpest resonance behavior that can be strongly weakened by the surface roughness. (e) Measured *J–V* characteristics of the colored semitransparent perovskite PV cell devices under simulated AM 1.5 solar spectrum illumination (100 mW cm^{-2}). Reproduced with permission [12]. Copyright 2015, Royal Society of Chemistry.

on the CIE 1931 chromaticity diagram with the different thickness of the Ag film in the optical cavity. Increasing the thickness of the Ag layer allows the color coordinates to move to the edge of the chromaticity diagram, which means that the color purity is enhanced. At positions of the transmission peak (445, 540, and 645 nm for the blue, green, and red colored PV cells) that corresponds to the resonant wavelength of the optical cavity, the field intensity is strongly concentrated in the a-Si photoactive layer as shown in figures 6(d)–(f). Such a strong field confinement in the WO_3 cavity layer is enabled within a very narrow bandwidth, which arises from very strong reflections from a fairly thick Ag film (40 nm). It is shown that the optical field intensity in the a-Si photoactive layer is lower at the resonant wavelengths because these wavelength components of visible light are not efficiently harvested by the PV cells to generate electric power but transmitted to create the desired semitransparent colors, whereas the intensity of the optical field in the photoactive layer at off-resonance wavelength regions is quite high, which is attributed to the strong reflections from the thick Ag layer, implying that most incident solar spectrum could be reflected back to the a-Si photoactive layer to contribute to the electricity generation. Although it is well-known that the optical properties of the traditional optical cavity are highly sensitive with respect to the incidence angle due to the cavity layer comparable to the wavelength of incident light, there are several ways to achieve the angle invariant performance by exploiting a flat dispersion characteristics that can be enabled by controlling the phase shift in a proper manner [48–52].

Since this design principle is fairly general, the presented scheme can be readily applied to other PV material system, including perovskite semiconductors, as described in figure 7 [12]. In figure 7(a), the device structure is schematically shown. For the photoactive layer, the organolead halide perovskite semiconductor, $CH_3NH_3PbI_{3-x}Cl_x$, is used due to its excellent absorption property in the visible region, which leads to high energy conversion efficiency in a planar device configuration. In order to produce the semitransparent colors, which can be easily tuned with the different thickness of the cavity medium (i.e. WO_3), the thickness of the perovskite material is designed to be fairly thin (80 nm) so that a portion of incident light can be used for the color generation. Such a thin photoactive layer is also beneficial to the efficient collection of photogenerated charges to the electrodes with suppressed charge carrier recombination, which is attributed to the fact that the designed photoactive layer thickness is much thinner than the charge diffusion length of the perovskite semiconductor [53, 54]. Figure 7(d) presents simulated and measured transmission spectra at normal incidence, and the optical images of the fabricated devices are shown in figure 7(c). It is observed that the red colored cell shows a large difference between the simulated and measured spectra as compared to other colored cells. This is because the red colored PV device has the resonance with the highest *Q*-factor (i.e. sharp transmission peak), which arises from the negligible absorption characteristics of the perovskite semiconductor material at longer wavelengths, and hence the surface roughness can produce more significant effects on the sharp resonance, making the resonance broad with reduced efficiency. The strong optical absorptions of the perovskite semiconductor at shorter wavelengths lead to the low transmission efficiency of the blue colored PV cell. The blue colored cell needs to transmit a small portion of incident light to produce the blue colors, which is not used to generate electricity, while the red colored cell can almost fully capture the shorter wavelengths where the perovskite semiconductor materials have strong optical absorptions, thereby yielding a high J_{sc} value. This can be validated by the increase in the J_{sc} from the blue colored cell ($J_{sc} = 6.89\,\mathrm{mA\,cm^{-2}}$) to the red colored cell ($J_{sc} = 7.63\,\mathrm{mA\,cm^{-2}}$) as presented in figure 7(e).

6. Discussion

Although diverse color filtering schemes can be readily applied to the existing PV systems to develop a new PV platform that offers a new functionality capable of creating desired colors, the power conversion efficiency is still limited as some portion of incident light needs to be utilized for the color generation. To further enhance the efficiency of the PV devices, the simple way is to combine with broadband AR coatings and novel light trapping structures at the nanoscale, such as metallic nanostructures and randomly textured surfaces, which can induce the light scattering and effectively increase the optical path length [55–59]. Other possible way to further improve the power conversion efficiency of the colored PV cells is to exploit the broadband light absorbing approaches at visible frequencies and the perfect light absorptions in the infrared (IR) region, the latter of which can potentially be applicable to the thermo-PV technologies [13–22].

One can also consider a tandem structure by exploiting semiconductors that can selectively harvest UV and IR parts of the spectrum, both of which are not visible to the human eye, while transmitting the visible light spectrum, thus leading to further increases in performance [42, 60–62].

Acknowledgments

These work are supported in part by the National Science Foundation, especially grant No. ECCS 1202046. HJP acknowledges the support by the Basic Science Research Program through the National Research Foundation of Korea (NRF), funded by the Ministry of Education (NRF-2014R1A1A2056403), and the Ajou University research fund. These works are also partially supported by the Ministry of Trade, Industry & Energy (MOTIE, 10051565) and Korea Display Research Corporation (KDRC) support program for the development of future devices technology for the display industry. The authors would like to thank Masanori Fukuda for his great contribution to the perovskite PV work.

References

[1] Ahmad S, Guillen E, Kavan L, Gratzel M and Nazeeruddin M K 2013 *Energy Environ. Sci.* **6** 3439
[2] Kumaresan D, Thummel R P, Bura T, Ulrich G and Ziessel R 2009 *Chem. Eur. J.* **15** 6335
[3] Park H J, Xu T, Lee J Y, Ledbetter A and Guo L J 2011 *ACS Nano* **5** 7055
[4] Lee J Y, Lee K T, Seo S and Guo L J 2014 *Sci. Rep.* **4** 4192
[5] Lee K T, Lee J Y, Seo S and Guo L J 2014 *Light Sci. Appl.* **3** e215
[6] Kats M A, Blanchard R, Genevet P and Capasso F 2013 *Nat. Mater.* **12** 20
[7] Lee K T, Seo S, Lee J Y and Guo LJ 2014 *Appl. Phys. Lett.* **104** 231112
[8] Kats M A *et al* 2012 *Appl. Phys. Lett.* **101** 221101
[9] Lee K T, Seo S, Lee J Y and Guo L J 2014 *Adv. Mater.* **26** 6324
[10] Chen Y H, Chen C W, Huang Z Y, Lin W C, Lin L Y, Lin F, Wong K T and Lin H W 2014 *Adv. Mater.* **26** 1129
[11] Lee K T, Lee J Y, Seo S and Guo L J 2015 *IEEE J. Photovolt.* **5** 1654
[12] Lee K T, Fukuda M, Joglekar S and Guo L J 2015 *J. Mater. Chem.* C **3** 5377
[13] Liu Z, Liu G, Liu X, Huang S, Wang Y, Pan P and Liu M 2015 *Nanotechnology* **26** 235702
[14] Liu Z, Liu X, Huang S, Pan P, Chen J, Liu G and Gu G 2015 *ACS Appl. Mater. Interfaces* **7** 4962
[15] Liu Z, Yu M, Huang S, Liu X, Wang Y, Liu M, Pan P and Liu G 2015 *J. Mater. Chem.* C **3** 4222
[16] Liu Z, Liu G, Fu G, Liu X and Wang Y 2016 *Opt. Express* **24** 5020
[17] Liu X, Liu G, Fu G, Liu M and Liu Z 2016 *Nanotechnology* **27** 125202
[18] Zhu P and Guo L J 2012 *Appl. Phys. Lett.* **101** 241116

[19] Hedayati M K, Javaherirahim M, Mozooni B, Abdelaziz R, Tavassolizadeh A, Chakravadhanula V S K, Zaporojtchenko V, Strunkus T, Faupel F and Elbahri M 2011 *Adv. Mater.* **23** 5410
[20] Lee K T, Ji C and Guo L J 2016 *Appl. Phys. Lett.* **108** 031107
[21] Yang C, Ji C, Shen W, Lee K T, Zhang Y, Liu X and Guo L J 2016 *ACS Photon.* in press (doi:10.1021/acsphotonics.5b00689)
[22] Aydin K, Ferry V E, Briggs R M and Atwater H A 2011 *Nat. Commun.* **2** 517
[23] Barnes W L, Dereux A and Ebbesen T W 2003 *Nature* **424** 824
[24] Genet C and Ebbesen T W 2007 *Nature* **445** 39
[25] Diest K, Dionne J A, Spain M and Atwater H A 2009 *Nano Lett.* **9** 2579
[26] Kolle M, Salgard-Cunha P M, Scherer M R J, Huang F, Vukusic P, Mahajan S, Baumberg J J and Steiner U 2010 *Nat. Nanotechnol.* **5** 511
[27] Park H J, Kang M-G and Guo L J 2009 *ACS Nano* **3** 2601
[28] Kang M G, Kim M-S, Kim J and Guo L J 2008 *Adv. Mater.* **20** 4408
[29] Kang M-G, Park H J, Ahn S H, Xu T and Guo L J 2010 *IEEE J. Sel. Top. Quantum Electron.* **16** 1807
[30] Kang M-G, Xu T, Park H J, Luo X and Guo L J 2010 *Adv. Mater.* **22** 4378
[31] Kang M-G, Park H J, Ahn S H and Guo L J 2010 *Sol. Energy Mater. Sol. Cells* **94** 1179
[32] Myong S Y, Kim S S and Lim K S 2004 *J. Appl. Phys.* **95** 1525
[33] Meyer J, Zilberberg K, Riedl T and Kahn A 2011 *J. Appl. Phys.* **110** 033710
[34] He Y, Chen H Y, Hou J and Li Y 2010 *J. Am. Chem. Soc.* **132** 1377
[35] O'Malley K M, Li C Z, Yip H L and Jen A K 2012 *Adv. Energy Mater.* **2** 82
[36] Hong K *et al* 2011 *J. Phys. Chem.* C **115** 3453
[37] Tian B, Williams G, Ban D and Aziz H 2011 *J. Appl. Phys.* **110** 104507
[38] Kim H, Lee K T, Zhao C, Guo L J and Kanicki J 2015 *Org. Electron.* **20** 103
[39] Winkler T *et al* 2011 *Org. Electron.* **12** 1612
[40] Eperon G E, Burlakov V M, Goriely A and Snaith H J 2014 *ACS Nano* **8** 591
[41] You P, Liu Z, Tai Q, Liu S and Yan F 2015 *Adv. Mater.* **27** 3632
[42] Chen C C, Dou L, Gao J, Chang W H, Li G and Yang Y 2013 *Energy Environ. Sci.* **6** 2714
[43] Bauer A, Wahl T, Hanisch J and Ahlswede E 2012 *Appl. Phys. Lett.* **100** 073307
[44] Lin P, Choy W C H, Zhang D, Xie F, Xin J and Leung C W 2013 *Appl. Phys. Lett.* **102** 113303
[45] Beiley Z M *et al* 2013 *Adv. Mater.* **25** 7020
[46] Zhang C, Zhao D, Gu D, Kim H, Ling T, Wu Y K and Guo L J 2014 *Adv. Mater.* **26** 5696
[47] Gu D, Zhang C, Wu Y K and Guo L J 2014 *ACS Nano* **8** 10343
[48] Economou E N 1969 *Phys. Rev.* **182** 539
[49] Shin H, Yanik M F, Fan S, Zia R and Brongersma M L 2004 *Appl. Phys. Lett.* **84** 4421
[50] Lee K T, Seo S and Guo L J 2015 *Adv. Opt. Mater.* **3** 347
[51] Park C S, Shrestha V R, Lee S S, Kim E S and Choi D Y 2015 *Sci. Rep.* **5** 8467
[52] Mao K, Shen W, Yang C, Fang X, Yuan W, Zhang Y and Liu X 2016 *Sci. Rep.* **6** 19289
[53] Stranks S D, Eperon G E, Grancini G, Menelaou C, Alcocer M J P, Leijtens T, Herz L M, Petrozza A and Snaith H J 2013 *Science* **342** 341
[54] Xing G, Mathews N, Sun S, Lim S S, Lam Y M, Grätzel M, Mhaisalkar S and Sum T C 2013 *Science* **342** 344
[55] Brongersma M L, Cui Y and Fan S 2014 *Nat. Mater.* **13** 451
[56] Guo C F, Sun T, Cao F, Liu Q and Ren Z 2014 *Light Sci. Appl.* **3** e161
[57] Atwater H A and Polman A 2010 *Nat. Mater.* **9** 205
[58] Mokkapati S and Catchpole K R 2012 *J. Appl. Phys.* **112** 101101
[59] Fukuda M, Lee K T, Lee J Y and Guo L J 2014 *IEEE J. Photovolt.* **4** 1337
[60] Lunt R R and Bulovic V 2011 *Appl. Phys. Lett.* **98** 113305
[61] Zhao Y, Meek G A, Levine B G and Lunt R R 2014 *Adv. Opt. Mater.* **2** 606
[62] Zhu R *et al* 2011 *ACS Nano* **5** 9877